

Analysis and compensation of the series resistance effects on the characteristics of ferroelectric capacitors

M. Massarotto¹, F. Driussi¹, M. Bucovaz¹, A. Affanni¹, S. Lancaster², S. Slesazek², T. Mikolajick^{2,3}, D. Esseni¹

¹DPIA, Università degli Studi di Udine, Via delle Scienze 206, Udine, Italy

²NaMLab gGmbH, Nöthnitzer Str. 64a, 01187 Dresden, Germany

³IHM TU Dresden, Nöthnitzer Str. 64, 01187 Dresden, Germany

Abstract: Ferroelectric device optimization requires a dependable characterization of the ferroelectric (FE) material. Here, we highlighted how series resistance (R_S) impacts the I-V characteristics of Metal-Ferroelectric-Metal (MFM) stacks with peculiar distortions, possibly leading to an inaccurate extraction of the FE parameters and a misleading interpretation of its switching dynamics. For the first time to our knowledge, we here propose a procedure for an improved extraction of the FE parameters even in presence of a significant series resistance.

Lead author: Marco Massarotto

DPIA, Università degli Studi di Udine

via delle Scienze, 206

33100, Udine, Italy

FAX: +39-0432558251

e.mail: massarotto.marco001@spes.uniud.it

Authors preference: ORAL PRESENTATION

Analysis and compensation of the series resistance effects on the characteristics of ferroelectric capacitors

M. Massarotto¹, F. Driussi¹, M. Bucovaz¹, A. Affanni¹, S. Lancaster², S. Slesazek², T. Mikolajick^{2,3}, D. Esseni¹

¹DPIA, University of Udine, Italy

²NaMLab gGmbH, Dresden, Germany

³IHM TU Dresden, Germany

Introduction. HfZrO₄ (HZO) is a CMOS-compatible, highly scalable ferroelectric (FE) raising interest for many applications ranging from memories to neuromorphic computing [1]. However, the FE device optimization requires an in-depth HZO characterization and a dependable extraction of its remnant polarization (P_R) and coercive voltage (V_C). Here we report an experimental study at different frequencies and for samples with different areas, evidencing the impact of the series resistance (R_S) on the extracted P_R and V_C values. We quantitatively assess the influence of R_S and propose a new compensation procedure for a dependable extraction of P_R and V_C also in presence of relevant R_S values.

Devices and experimental setup. Metal-Ferroelectric-Metal (MFM) stacks are fabricated by ALD of 10.5 nm HZO onto W (30 nm)/TiAlN (22 nm) bottom electrode (BE, Fig.1). PVD is used for the 22 nm TiAlN top contacts. Circular areas with diameter $\Phi=110\div450\ \mu\text{m}$ are defined by shadow mask evaporation of Ti/Pt and etching. The BE is reached through a lateral broken MFM device (BD, Fig.1). To measure the samples, the verified setup in Fig.1 is used [2]. FE polarization P is switched by a triangular voltage wave (V_{IN} , Fig.2a) and studied by measuring the switching current I_{MFM} during time (Fig.1). Then, the I_{MFM} integral provides the switching charge, which is interpreted as P [3].

Experiments. Triangular V_{IN} pulses result in I_{MFM} peaks due to P switching, which add to the V_{IN} independent dielectric response (Fig.2) [3]. Fig.2 shows I_{MFM} and the P-V curves of a sample with $\Phi=110\ \mu\text{m}$. Two V_{IN} frequencies (f) are shown and we verified the proportionality between I_{MFM} and f , while P is independent of f . Thus, in the following, we report I_{MFM} normalized to both f and device area to compare different samples and measurement conditions. Fig.3 shows results for a 450 μm sample. At 10 kHz, the normalized I_{MFM} (red) is largely distorted compared to 100 Hz (black), showing a shift in voltage and a reduction of the normalized peak (the absolute peak value, I_{pk} , is larger at 10 kHz, Fig.3b). The resulting P-V loop at 10 kHz tends to widen and the coercive voltages increase (Fig.3c). This may suggest that FE cannot track V_{IN} [4]. To study this point, we measured many samples with different Φ over f (0.1 \div 10 kHz). We then defined the coercive voltages V_C^+ , V_C^- at the current peaks (Fig.3a), while the $2P_R$ value was obtained from the P-V loops (Fig.2c). Fig.4(a) shows the box plot of all $2P_R$ values, which are rather flat over f , indicating a complete FE switching irrespective of f and Φ . Fig.4(b) reports the average V_C^+ , V_C^- grouped by device area, showing that $|V_C^\pm|$ increase with f and especially for the larger Φ , thus indicating that this trend could be an extrinsic, spurious effect. In fact, I_{pk} increases with Φ and f (Fig.3b), suggesting a possible impact of a series resistance R_S .

Series resistance effect. We verify the hypothetical R_S effect on the MFM curves through the experiment in Fig.5. A 110 μm MFM is first measured at $f=100\ \text{Hz}$ (black), resulting in the lowest possible I_{MFM} (small Φ , low f) and thus the minimum R_S influence. Then, we repeated the measurement by inserting an external resistance R_{ext} in series with the MFM. The I-V curve (Fig.5, red) is now distorted, showing a I_{MFM} peak decrease and a $|V_C^\pm|$ modulation very similar to those seen in larger samples measured at high f (Fig.3). This confirms that such distortion can be partly due to R_S .

We estimated the contributions to R_S by measuring the resistance between several broken devices through AC analysis (Fig.6), obtaining $R_S\approx 200\ \Omega$, that is non-negligible even for the smallest samples when measuring at 10 kHz. So R_S induces a voltage drop that distorts the V_{FE} waveform actually delivered to the MFM (Fig.7a, red), especially at the switching peaks of I_{MFM} . Of course, the voltage drop on R_S depends on the I_{MFM} value, thus on Φ and f . We estimate the actual V_{FE} through Eq.1 (Fig.8), the measured I_{MFM} and the R_S calculated from results in Fig.6. Then we re-plot I_{MFM} and P versus V_{FE} in Figs.7(b) and (c), respectively (solid lines). Now, the P-V loop at 10 kHz (red) is consistent with that measured at 100 Hz (black), thus indicating that the P-V alteration at 10 kHz was an artifact due to R_S .

However, even if such re-scaling of the voltage x -axis seems to restore the P-V hysteresis, it is not sufficient to match the I-V curves at different f (Fig.7b) [5]. Indeed, the coercive voltages at 10 kHz (solid red) are now much closer to those at 100 Hz (black), but the I_{MFM} peaks (normalized to Φ and f) still remain lower at high f (the y -axis is not affected by the re-plotting). This is because the switching and thus I_{MFM} depend also on the actual V_{FE} waveform, which differs significantly for the two f values (see Fig.7a). Hence, we devised a procedure to eliminate the R_S influence even on the I-V characteristics. Fig.7(a,c) indicates that P does not depend on the V_{FE} slew rate. So in Eq.2 of Fig.8, we define the large-signal capacitance C_{LS} linking P to V_{FE} [6]. Eq.3 now elaborates the measured I_{MFM} data, obtaining C_{LS} that is invariant w.r.t. the V_{FE} time evolution and unaffected by the R_S effect. We validated the method by simulating a ferroelectric capacitor with different in-series R_S values (Fig.9). Simulated I_{MFM} (a) shows the same features observed in experiments (Fig.3a). The application of Eq.3 to the simulated I_{MFM} provides a unique C_{LS} - V_{FE} curve, cleaned from the R_S distortion, thus validating the method. Then, we applied Eq.3 to the experiments. Fig.10 shows that, by accounting for R_S in Eqs.1 and 3, we obtain the same C_{LS} - V_{FE} curve, irrespective f , thus suggesting that the I_{MFM} distortions are mainly due to R_S in the explored f range. Then, we calculate the P-V and I-V curves in Fig.11 with Eqs.4 and 5 and extract again the V_C^\pm and $2P_R$ values. Note that the corrected I-V curves in Fig.11(a, solid) completely recover from the distortions seen in the measured I_{MFM} (dashed). The correction method is finally applied to all measurements and the results are summarized in Fig.12. V_C^\pm values are now independent of both Φ and f .

Conclusion. Series resistance effects on MFM curves are here assessed. For the first time, a rigorous procedure to compensate for R_S is presented. A large-signal capacitance is calculated and used to extract $2P_r$ and V_C^\pm , whose values are frequency-independent in the explored f range [7]. This study reveals that HZO has a high switching speed and the increase of the coercive voltages at large f is to a large extent due to spurious effects of unwanted series resistances [8].

Acknowledgments. This work is funded by the European Union through the BeFerroSynaptic Project (GA: 871737).

- [1] S. Slesazek et al., *Nanotechnology*, vol. 35, p. 352003, 2019.
 [2] M. Massarotto et al., *Solid State Elec.*, vol. 194, p. 108364, 2022.
 [3] M. Massarotto et al., *Solid State Elec.*, vol. 200, p. 108569, 2023.
 [4] X. Lyu et al., *Symposium on VLSI Tech.*, pp. T44-T45, 2019.
 [5] Z. M. Gao et al., *Jour. of Semiconduc.*, vol. 43, p. 014102, 2022.
 [6] M. Massarotto et al., *Proceedings of ICMTS*, pp. 170-175, 2023.
 [7] P. Hao et al., *Adv. Functional Mater.*, vol. 33, p. 2301746, 2023.
 [8] S. Boyn et al., *Applied Phys. Lett.*, vol. 109, p. 232902, 2016.

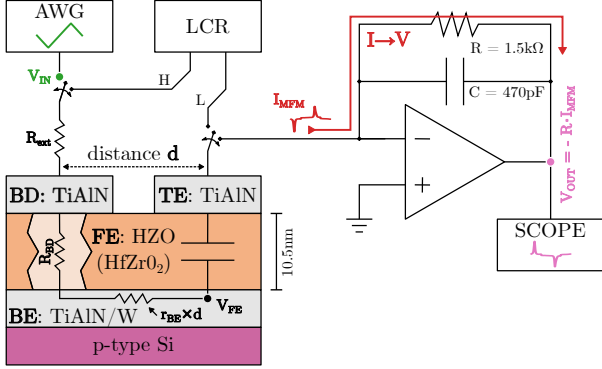


Figure 1: Experimental setup used for the MFM characterization. The setup is used as an I→V converter to probe the switching current I_{MFM} . The Arbitrary Waveform Generator (AWG) drives the MFM sample and V_{OUT} is monitored through an oscilloscope. The setup includes also an LCR meter for AC characterization [6] and the possibility to insert an external resistance R_{ext} in series with the MFM sample.

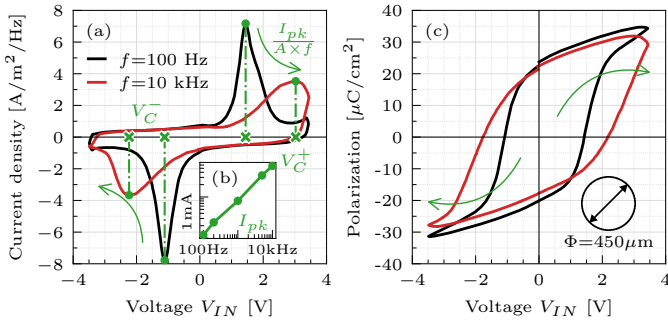


Figure 3: (a) I_{MFM} normalized over frequency as a function of V_{IN} of a MFM with $\Phi = 450 \mu\text{m}$. At $f = 10 \text{ kHz}$ the I-V curve is largely distorted. (b) Absolute peak current versus f . (c) P-V curves obtained from the I-V characteristics in (a), also showing the distortion at $f = 10 \text{ kHz}$.

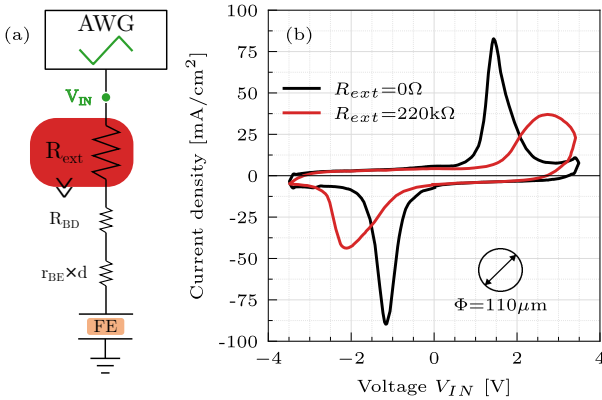


Figure 5: I_{MFM} measured for a MFM sample with $\Phi = 110 \mu\text{m}$ at $f = 100 \text{ Hz}$. This experiment ensures the lowest possible current. (a) I_{MFM} is measured with or without the insertion of a large external series resistance R_{ext} . (b) The series resistance effect is evident, with an I_{MFM} distortion (red) very similar to those observed in large samples measured at high f (Fig.3a).

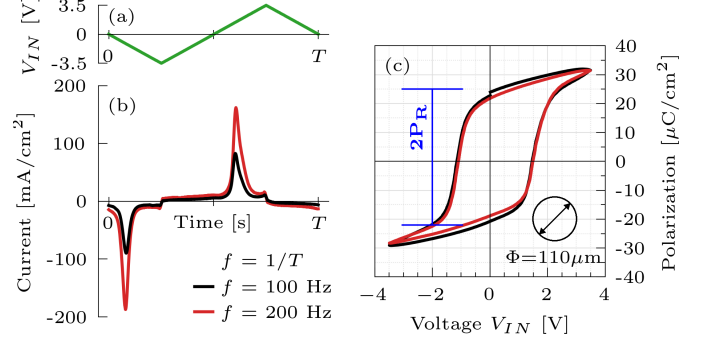


Figure 2: Input triangular voltage (a) used to switch the MFM stacks. Pulses with frequencies f ranging from 100 Hz to 10 kHz are used to obtain the switching current (b) of the MFM samples. Note that I_{MFM} is proportional to f . (c) P-V characteristics for an MFM with $\Phi = 110 \mu\text{m}$ obtained by integrating the current curves in (b). $2P_R$ is defined in the figure.

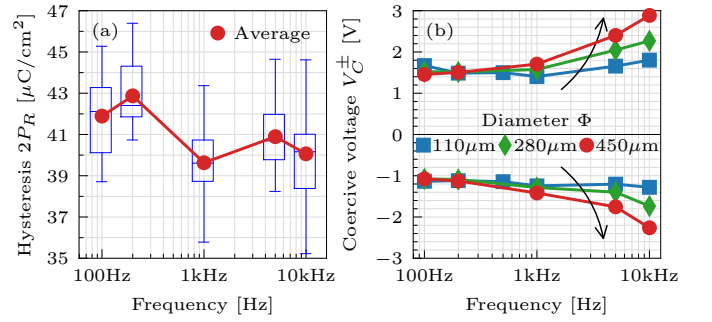


Figure 4: (a) Box plot of extracted $2P_R$ values for all the measured samples. The average $2P_R$ seems independent of f , indicating a full switching of all devices. (b) Average coercive voltages V_C^+ (top) and V_C^- (bottom) versus f for different device areas. Their magnitude increases with f suggesting a slow response of the MFM at large f . The dependence on the device area is also evident.

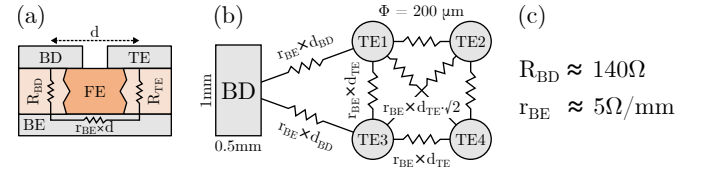


Figure 6: The contributions to R_S (a) are estimated by measuring the resistance seen between several broken MFM samples (b) by means of the LCR meter in Fig.1. R_{BD} is the resistance associated to the access device generally used for the MFM characterization, while R_{TE} is the resistance of the specific broken MFM. r_{BE} is the resistance per unit length of the bottom electrode. The crossing of the different resistances measured in (b) allows us to obtain the values in (c) that are then used to calculate the R_S value of the specific MFM under test as $R_S = R_{BD} + r_{be} \cdot d$, where d is the distance between the access device BD and the MFM sample.

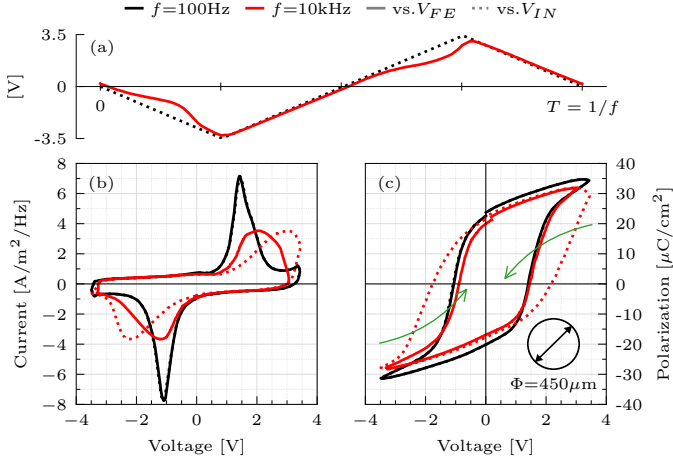


Figure 7: (a) Time evolution of the applied V_{IN} (dashed black) and of the voltage drop across the MFM (V_{FE} , red) when measuring a $450\mu\text{m}$ sample at 10kHz . (b) Measured I_{MFM} - V_{IN} (dashed) and I_{MFM} vs. V_{FE} (solid) calculated with Eq.1 in Fig.8 for two f values. (c) Calculated P - V_{IN} (dashed) and P - V_{FE} (solid) curves for two f values.

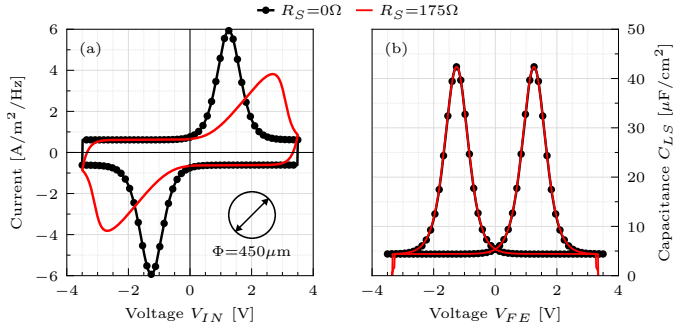


Figure 9: Circuit simulations of a hysteretic capacitor with (red) or w/o (black) the insertion of a series resistance R_S . (a) Simulated I-V curves highlight the R_S impact on the MFM characteristics (shift and lowering of switching peak), which is exactly what we observe in the experiments of Figs.3(a) and 5. (b) By using Eq.3 of Fig.8, we obtain a unique large-signal capacitance for the MFM stack, irrespective of R_S , thus validating the proposed correction method.

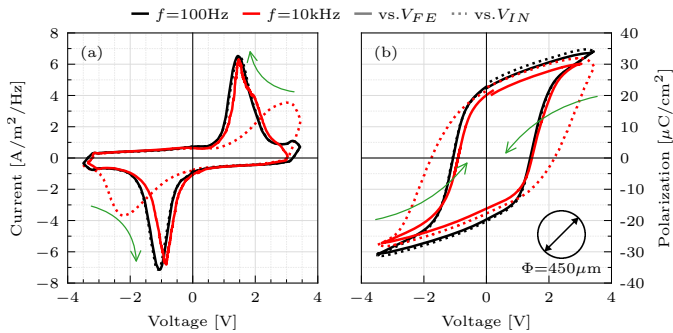


Figure 11: (a) I-V curves measured at two f values. Dashed lines are the measured I_{MFM} - V_{IN} characteristics, solid lines are the I_{corr} - V_{FE} curves obtained through Eqs.1 and 5. Note how the corrected current completely recovers from the distortions due to R_S , leading to a unique I-V curve for all frequencies. (b) Original (dashed) and corrected (solid, Eq.4) P-V loops. Again, despite the R_S impact, the correction procedure allows us to recover a unique MFM characteristic, irrespective of the measurement frequency.

$$V_{FE} = V_{IN} - R_S \cdot I_{MFM} \quad (1)$$

$$I_{MFM} = \frac{dP(V_{FE})}{dt} = \frac{dP}{dV_{FE}} \cdot \frac{dV_{FE}}{dt} = C_{LS} \cdot \frac{dV_{FE}}{dt} \quad (2)$$

$$C_{LS}(V_{FE}) = I_{MFM} \cdot \left(\frac{dV_{FE}}{dt} \right)^{-1} = I_{MFM} \cdot \left(\frac{dV_{IN}}{dt} - R_S \frac{dI_{MFM}}{dt} \right)^{-1} \quad (3)$$

$$P = \int C_{LS}(V_{FE}) dV_{FE} \quad (4)$$

$$I_{corr} = C_{LS} \cdot \frac{dV_{IN}}{dt} = I_{MFM} \cdot \left(1 - R_S \frac{dI_{MFM}}{dV_{IN}} \right)^{-1} \quad (5)$$

Figure 8: Equations used to correct the MFM characteristics affected by R_S . The model assumes that the polarization depends only on the V_{FE} value applied to the MFM stack, irrespective of the V_{FE} time evolution, as suggested by the P-V loops in Fig.7(c, solid).

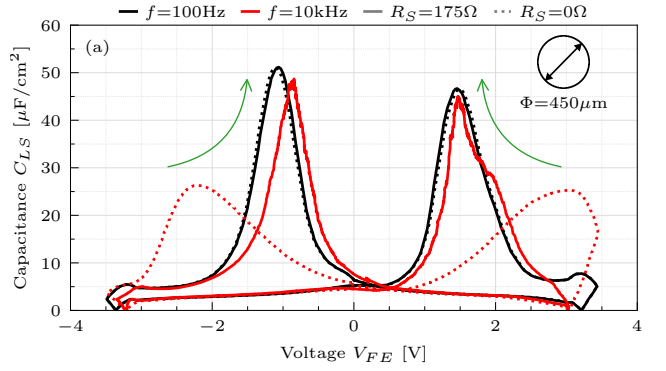


Figure 10: Large-signal capacitance C_{LS} calculated with Eq.3 and the I_{MFM} measured on a $450\mu\text{m}$ sample for two f values. *Dashed*: C_{LS} - V_{FE} curve obtained using $R_S = 0$ in Eqs.1 and 3. *Solid*: C_{LS} - V_{FE} curve obtained for $R_S = 175\Omega$ (compatible with the analysis in Fig.6). By accounting for the R_S impact, a unique C_{LS} - V_{FE} curve for the different f values is obtained. Note that the C_{LS} peak can be used to monitor V_C^\pm and to obtain the correct P-V loops.

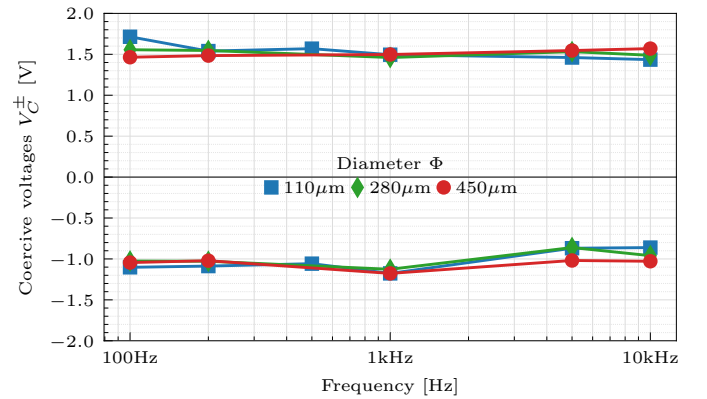


Figure 12: Average V_C^+ and V_C^- values obtained after applying the correction procedure to all measurements performed on the MFM samples. Thanks to the correction, the V_C^\pm magnitudes are now rather flat in frequency and independent of the device area.